JCRMHS

Journal of Clinical Case Reports, Medical Images and Health Sciences

Volume 5 Issue 2, 2023

Article Information

**Received date:** 01/06/2023

**Published date:** 24/07/2023

*Corresponding author

*Etcheverry, Centro de Investigaciones Ópticas (CCT-CONICET La Plata, UNLP and CIC-BA), Gonnet, La Plata, Argentina.

*Key Words:

Non-melanoma skin cancer, one-point fluorescence detection, violet LED lamp.

Original Research

# Applications in Light-induced Spectroscopy with violet LED lamp: Autofluorescence

M.E. Etcheverry[1,3]*, M.A Pasquale[2,3]**, M. Garavaglia[1,3]

*[1]Centro de Investigaciones Ópticas (CCT-CONICET La Plata, UNLP and CIC-BA), Gonnet, La Plata, Argentina.*

*[2]Instituto de Investigaciones Fisicoquímicas Teóricas y Aplicadas (CCT-CONICET La Plata, UNLP and CICBA), La Plata, Argentina.*

*[3]Facultad de Ciencias Exactas, Universidad Nacional de La Plata, Argentina.*

## Abstract

The main objective of the present study was to develop a violet LED light source suitable for medical application devoted to the diagnostic and treatment of non-melanoma skin cancers. For this propose, we constructed a 12 W violet LED lamp (with maximum emission peak at 405 nm) made up of four mobile 3 W LED. The LED lamp was characterized employing a spectrometer coupled to an optical fiber. The irradiance, the radiant power and the radiant intensity for different distances between the lamp and the detector was assessed. Data were compared with a simulated LED lamp by using the Zemax optic software for the realization of luminaries with the desired characteristics as required for medical applications.

The developed lamp in combination with a portable spectrometer was employed under medical supervision to detect differences in the emission spectrum of skin suspicious regions and healthy ones of a patient with non-melanoma skin cancer. The light of the LED lamp was concentrated in the examined region by means of the proper focusing of the four individual LEDs, rendering a high intensity homogeneous spot. Thus, endogenous chromophores at the skin were excited, and the emission intensity appeared to be enough to detect an enhanced peaked structure around 600 nm for some suspicious regions before treatment, and that were absence in healthy regions. These differences can be related to the augmented protoporphyrin IX content in neoplastic regions.

Results presented in this work indicates the usefulness of the developed LED lamp as an easyto-use device for the non-invasive detection of skin neoplastic pathologies, before and after treatment, with the aim of better define the malignant regions as well as predict the outcome of a certain treatment.

## Introduction

The early detection of a neoplastic disease, as well as the development of more efficient treatments, are crucial for improving the survival rate. A variety of new and emerging diagnostic strategies based on spectroscopic techniques such as non-invasive one-point fluorescence (PF) detection, are available to improve the screening procedure [1,2]. PF technique provides useful information for monitoring the evolution of the abundance and distribution of endogenous fluorophores associated with the neoplastic disease in low-pigmented superficial neoplasia [3,4].

Currently, the use of devices emitting light is an indispensable element of many non-invasive diagnostic procedures. Non-invasive fluorescence detection techniques are available for point measurement which provides information useful for monitoring the abundance and location of the fluorophores in lowpigmented superficial neoplasia. These fluorophores could be classified into three main categories: endogenous fluorophores that are responsible for



DOI: 10.55920/JCRMHS.2023.05.001203

native tissue fluorescence (autofluorescence) like keratin, porphyrins, vitamins and lipids [1,3,5-8]; fluorophores synthetized in the tissue after external administration of a precursor molecule, specifically protoporphyrin IX (PpIX) induced by 5aminolevulinic acid (ALA) [9]; and fluorophores administrated as exogenous drug such as tetra(mhydroxyphenyl) chlorin (mTHPC), a typical photosensitizer used in photodynamic therapy (PDT) [10]. In this case, because of the optimal dose during and after PDT are extremely variable [2], the prognosis of PDT treated patients is required. In this vein, it has been reported that fluorescence measurements of PpIX in the skin of patients showed changes in PpIX levels during therapy (photobleaching) and was a good predictor of clinical results [11].

The influence of tissue optics on fluorescence measurements were comprehensively reviewed in literature [12]. Thus, there are important properties that influence fluorescence measurements in tissues, namely, attenuation of light in the tissue, presence of endogenous fluorophores which cause autofluorescence, absorption, scattering, and reflection of light. Light-induced autofluorescence spectroscopy is a very attractive tool for early diagnosis of cancer due to its high sensitivity, easy-to-use methodology for measurements, lack of need for contrast agents' application on the tissue under investigation, possibilities for real time measurements and non-invasive tumor detection [3, 5]. This procedure allows the discrimination between pathological and normal tissue regions based on the differences in the content and metabolic state of a fluorescent compound. Fluorescence measurements are, in principle, straightforward. By filtering the reflected excitation light, it is possible to obtain rather strong signals from the tissues. Problems arise for interpreting the fluorescence signal as the fluorescence peaks are mostly broad and various fluorophores can overlap. Different optical properties in excitation and detection wavelengths also influence the signal. Furthermore, for the excitation wavelength range, generally in the UV region, the penetration depth is a few hundred micrometers, while for detection, the visible region is used, and light can go more than a couple of millimeters. These facts suggest that the intensity of fluorescence cannot be directly interpreted as the corresponding fluorophore concentration. Another consequence is that the measurement configuration, both in excitation and detection, strongly influences not only the signal level but also the shape of the spectrum. Moreover, when the lesion is highly pigmented the obtained fluorescence signal is too weak to be used for diagnostics. In such cases exogenous fluorescent markers could be applied [12,13].

In this work, we develop a violet LED light source suitable for medical application devoted to the diagnostic and treatment of non-melanoma skin cancers. The developed lamp, in combination with a portable spectrometer, is employed to detect differences between the emission spectrum of skin regions with non-melanoma skin cancer and healthy ones at the head of a patient.

## Materials and Methods

### Software for the LED lamp modeling

ZemaxOpticStudio 18.4.1 is a commonly used optical design program used for lighting systems design and image analysis [14-17]. Finished designs of optical devices can be exported as manufacturing-ready results such as ISO drawings and common CAD file formats. We simulated the LEDs source utilizing Blender 2.76 to create a three-dimensional model of the lens and the ZemaxOpticStudio 18.4.1 to describe the light emission performance. For this purpose, the following variables were considered: numbers of simulated rays (n), distance between the source and the sensing surface (d), dimension (12 cm x 12 cm) and number of pixels on the sensing surface (100 x 100 pixels), emission wavelengths of the source, its output power (W), and the light diffusion considered through the Lambertian fractions (1/10, 1/12, 0.55/1). Furthermore, we set the wavelength profile for the light source with a central maximum that falls off following a Gaussian curve. Results from simulations were utilized for guiding the LED lamp construction and then the outcome of the real and simulated lamps were compared.

### LED lamp construction and its photometric/ radiometric characterization

The LED lamp was constructed employing four 3 W LEDs, coupled to individual lenses and heat sinks. Each LED is fed by an independent electrical circuit with variable electric power to modulate the light intensity.

To characterize the constructed LED lamp, illuminance/ irradiance parameters such as irradiance (W/cm2), radiant power (W) and radiant intensity (W/sr) were determined. For this purpose, an AvaSpec-ULS3648-USB2-UA-25 spectrometer with a CCD detector (3648 pixels) provided with a DUV3648 filter for reduction of second-order effect, and coupled to an optical fiber (200 µm in diameter and 2 m in length) for UV / VIS / NIR range (250- 2500 nm), was utilized. A cosine law CC-VIS / NIR diffuser was adapted to the fiber optic lens. The signal was registered by Avasoft-Full Software. The optical fiber couple to the spectrometer was located at one end of an optical bench, and the light source at a known distance, at the other end of the bench (Fig.1).

### Spectroscopic measurements on the skin of a patient

The lesions on the skin are registered employing a point



DOI: 10.55920/JCRMHS.2023.05.001203

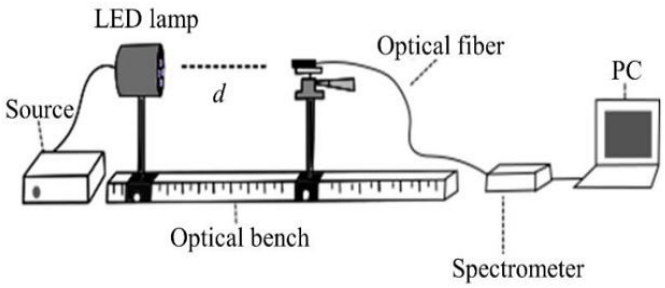


***Figure 1:*** *Scheme of the experimental arrangement for characterizing the LED lamp. At one end of the optical bench the LED source is located, and the tip of the fiber optic connected to the spectrometer, is placed at the other end, at a known distance. The spectrometer records the illuminance and allows expressing radiometric analogue units.*

monitoring system. The excitation light come from the violet LED source developed, and the detection is made by an optical fiber measuring in the 300-800 nm range. The fiber during measurement is supported by hand on the surface of the targeted detection tissue (Fig.2.). For comparison, emission spectra from suspicious skin regions, as well as healthy zones were registered.

## Results and Discussion

### Light source Modeling

The final light pattern generated by a LED is the result of the sum of the light directly refracted by the encapsulating lens, the light internally reflected inside the lens, and the light from the reflecting cup [20]. The first step to carry out the simulation is to build the emitting source based on a LED and the corresponding lens. Thus, an 8 ° lens was designed using the Blender 2.76 program. In this software, by drawing the profile of the lens and using the tool "spin", a solid of revolution was created. The draw lens was exported as CAD file to ZemaxOpticStudio where PMMA for lens material, Lambertian lens type (Lambertian fraction) [18], number of

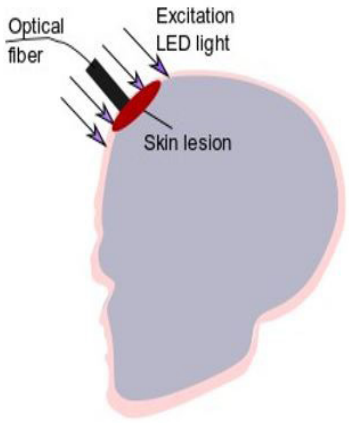


***Figure 2:*** *Scheme of autofluorescence point monitoring system: the excitation is external to the detector, and the detected emission light travels apart through an optical fiber. .*

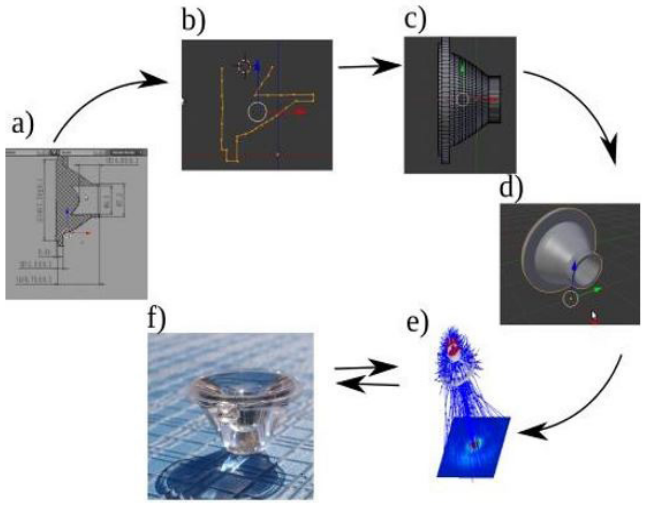


***Figure 3:*** *Converging lens design: a) Schematic drawing from lens data sheet; b) drawing the profile using the Blender 2.76 program; c) Application of spin tool to obtain the solid of revolution of the profile drawn in b); d) simulated lens with better definition than c), which was exported to Zemax; e) system of lens-LED in Zemax, and analysis of the emission on a detector surface located at 20 cm of the LED; f) photograph of the real lens.*

incident rays (n), wavelength, source-surface distance, and power, were specified. A scheme of the design process can be seen in Fig.3.

Blender 2.76 program; c) Application of spin tool to obtain the solid of revolution of the profile drawn in b); d) simulated lens with better definition than c), which was exported to Zemax; e) system of lens-LED in Zemax, and analysis of the emission on a detector surface located at 20 cm of the LED; f) photograph of the real lens.

Multiple variations were tested to model the exit beam of the light source. For example, the radiant intensity is represented for different variables (Fig.4). For n = 50.000 and Lambertian fraction 1/10, the image achieves acceptable definition on the detector surface (Fig.4c).

### Construction of the LED lamp

Each 3 W LED coupled to a heat sink and a lens was mounted on a mobile arm which can be displace in order to focus the lens-LED-heat sink systems on a convenient small region (Fig.5).

The real image of the illumination area generated by the LED source with central axis-oriented lenses at 20 cm distance, is shown in Fig.5e.

### Comparison between simulated and constructed LED lamp

We obtained the simulated irradiance from the source ($W/cm^2$) for different Lambertian fraction and compared it with the irradiance of the constructed LED lamp measured with the spectrometer described above. For a Lambertian



DOI: 10.55920/JCRMHS.2023.05.001203

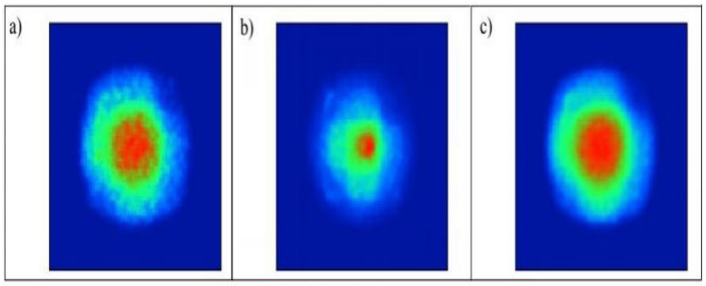


***Figure 4:*** *Radiant intensity for different n and Lambertian fractions for d = 20 cm and detector area 12 cm x 12 cm, i.e., 100 x 100 pixels: a) n = 10,000, Lambertian fraction: 1/10; b) n = 50,000, Lambertian fraction: 0.55 / 1; c) n = 50,000, Lambertian fraction: 1/10.*

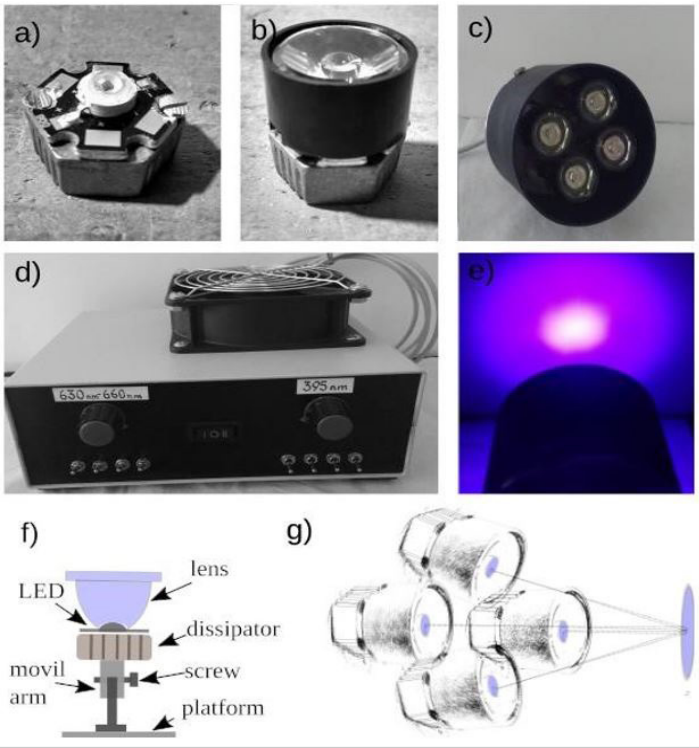


***Figure 5 :*** *Construction of the LED source with a maximum total power of 12W achieved with four 405 nm-LEDs of 3 W each. a) LED-heat sink system., a 3W high power LED is coupled to a single heat sink; b) Lens-LED- heatsink system, made up of a lens of 8◦ coupled to the LED-heat sink system; c) photograph of the 12W LED lamp with all four lens-LED-heat sink systems; d) 12W LED lamp power supply, with the possibility of turning on one, two, three or four LEDs simultaneously. Furthermore, it is possible to regulate the intensity of each LED and thus the overall source output; e) photograph of the constructed source with four focused LEDs illuminating a perpendicular surface; f) scheme of a single LED system consisting in a LED with an 8-degree lens coupled to the LED-heat sink on a mobile arm; g) Scheme of the four focused LEDs.*

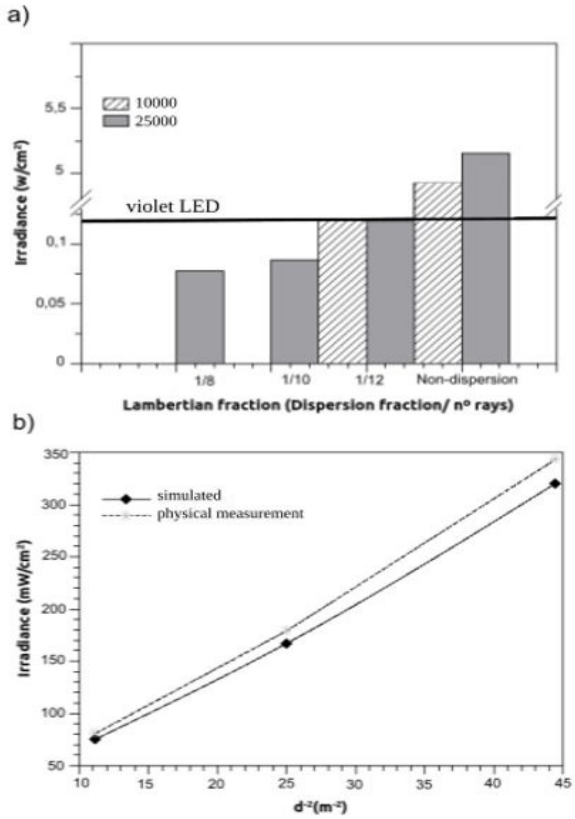


***Figure 6:*** *a) Irradiance for different Lambertian fractions. Comparison between the simulated violet LED lamp (vertical bars) with the physical measurement (horizontal line); b) Comparison between simulated and measured irradiance as a function of 1 / d2 for the LED lamp*

fraction 1/10, simulated results did not fit experimental observations, but changing it to 1/12, experimental data could be reproduced (Fig. 6a). An appropriate agreement was obtained between the simulation and the experiment in verifying the inverse-squared law, by measuring the irradiance for different distances (d) between the detector and the LED lamp with the experimental arrangement depicted in the scheme showed in figure 1 (Fig. 6b).

**Application of the violet LED source to detect non-melanoma skin cancer**

As know, the PpIX exhibits maximum light absorption (the Soret peak) at 405 nm and an emission peak in the red region. PpIX concentration is expected to be increased in pathological skin [21]. For this propose, we used the constructed violet LED lamp with maximum excitation peak at 405 nm to illuminate suspicious points in the head of a patient with a non-melanoma skin cancer before (Figure 7a) and after (Figure 7b) the treatment with a red medical laser emitting at 652 nm.

The fluorescence intensity of the PpIX was recorded with a spectrometer couple to an optical fiber with the scheme showed in figure 2. The average spectrum from suspicious



DOI: 10.55920/JCRMHS.2023.05.001203

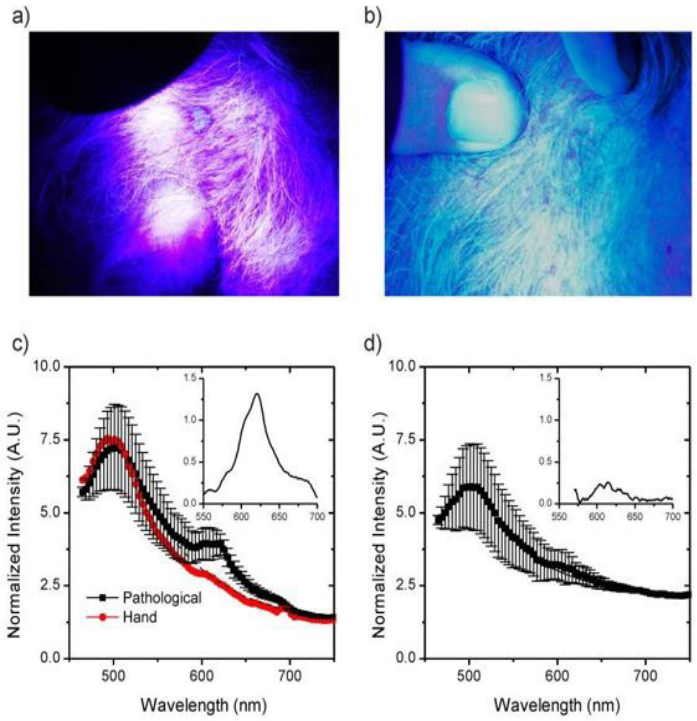


***Figure 7:*** *(a and b) Photographs of the lesion at the head of a patient before (a) and after (b) the treatment with a clinical red laser source. (c) Average fluorescence spectrum from lesions before treatment (black circles), and fluorescence spectrum from the skin of the hand (red circles) taken as healthy skin. The reference curve obtained from the decaying tail of the peak at 505 nm is shown in dashed lines. (d) Fluorescence spectrum from treated lesions. After subtracting the reference curve, a rather clear peak in the 600 – 700 nm range related to an increased amount of PpIX in untreated pathological regions, can be distinguished in comparison to treated ones, as depicted in the insets.*

areas as well as regions of healthy skin exhibits an emission peak at 505 nm, being the intensity of suspicious points greater than healthy skin area. Furthermore, suspicious points exhibit another structured peak in the 600 - 700 nm range (Fig. 7c, black squares). The later feature appears as a shoulder for the case of the average emission spectrum taken from the hand skin (Fig. 7c, red squares) or from different treated points at the head (Fig. 7d). A reference curve can be obtained from the decaying tail of the peak at 505 nm to be subtracted from emission intensity at the 550 – 700 nm range [22]. The inset in Fig. 7d shows a rather clear peak, while a noisy signal is obtained for red laser treated regions (inset in Fig. 7c). This description is consistent with the increased amount of PpIX in pathological regions in comparison with a healthy skin and treated regions. A similar interpretation has been proposed in literature [23].

Fluorescence spectroscopy with 405 nm excitation for the detection of non-melanoma tumors in vivo has been reported in literature [4]. In this work, authors have demonstrated the correlation between cancer detection diagnostic accuracy and skin phototype of the patient. With increasing of cutaneous pigmentation, the diagnostic accuracy for tumor detection and differentiation from normal skin fall down. In our case, we followed the fluorescence on a patient with non-melanoma neoplastic disease before and after the treatment. It can be detected a significant decrease in the fluorescence in the 600 – 700 nm range, for treated regions (Figure 7). We employed a point monitoring system like that employed in reference [24]. There, the pharmacokinetics of PpIX in skin tumors, i.e., basal cell carcinomas (BCC) and T-cell lymphomas, as well as in normal skin has been studied utilizing red (652 nm) laser induced fluorescence for the in vivo monitoring. Results from this research showed that the emission spectra indicated the build-up of the PpiX and the tumor selectivity in the superficial layers of the area planned for treatment.

## Conclusion

At present, histochemical methods are the standard procedures in diagnosis of many disorders, primarily neoplastic ones. However, autofluorescence-based techniques applied to tissue analysis can be performed in real time because it does not require any treatment of fixing or staining of the tissue. Most authors, who used autofluorescence in diagnostics of precancers and malignant tumors, have declared as drawbacks, that there was relatively high rate of false-positive findings [25-27]. These unexpected false positive may be caused by the appearance of a minimal amount of blood (hemoglobin) on surface, bacterial colonization [26], inflammation, edema, as well as scar formations. In any case, autofluorescence based strategies, due to their easy implementation in the clinic, are convenient for screening purpose.

In this work we describe the modeling, the construction and characterization of a violet LED light source with controlled power, and which can be focused on a small surface region, achieving and irradiance of

165 mW cm-2 at 25 cm from the source. Furthermore, the application of the LED source to the follow up of a non-melanoma skin cancer was reported. The fluorescence spectra from tumors and normal surrounding tissue regions illuminated by the developed UV/violet LED lamp, was registered employing a portable spectrometer and an optical fiber probe. Autofluorescence spectra were recorded pre- and pos-treatment with a clinical laser source. PpIX enhanced concentration was detected in pathological skin areas according to corrected fluorescence spectra, in agreement with the literature [28].

The present work suggests that changes in the fluorescence spectrum characteristics could be mainly relate to appearance or concentration changes in fluorophores, which are present in a skin pathology, and



DOI: 10.55920/JCRMHS.2023.05.001203

could be associated to changes in the metabolic activity, as concluded in the reference [29]. These results would be valuable in the design of photodynamic diagnostic protocols as well as for improving the control of PDT treatment dosing, rendering this alternative approach, either as a single or as an adjuvant intervention, more attractive for clinical massive application.

**Acknowledgement**: This work was supported by the Consejo Nacional de Investigaciones Científicas y Técnicas (CONICET, Argentina) and Universidad Nacional de La Plata (Grant No. 11/X900). M.A.P. is staff member of CONICET.

## References

1. Liu Q. Role of Optical Spectroscopy Using Endogenous Contrasts in Clinical Cancer Diagnosis. World J Clin Oncol 2011; 10: 50-63.
2. van Straten D, Mashayekhi V, de Bruijn HS, Oliveira S, Robinson DJ. Oncologic Photodynamic Therapy: Basic Principles, Current Clinical Status and Future Directions. Cancers (Basel) 2017; 9(19):2-54.
3. Borisova E, Avramov L, Pavlova P, Pavlova E, Troyanova P. Qualitative Optical Evaluation of Malignancies Related to Cutaneous Phototype. Proc. SPIE –Dynamics and Fluctuations in Biomedical Photonics VII 2010; 75630X.
4. Panjepour M, Julius C, Phan M, Vo-Dinh T, Overholt S. Laser-induced Fluorescence Spectroscopy for in vivo Diagnosis of Non-melanoma Skin Cancers. Lasers Surg Med 2002; 31: 367-73.
5. Bigio J, Mourant JR. Ultraviolet and Visible Spectroscopies for Tissue Diagnostics: Fluorescence Spectroscopy and Elastic-scattering Spectroscopy. Phys Med Biol 1997; 42: 803-14.
6. Na R, Stender I, Wulf H. Can Autofluorescence Demarcate Basal Cell Carcinoma from Normal Skin? A Comparison with Protoporphyrin IX Fluorescence. Acta Derm Venerol 2001; 81:246-49.
7. Pena A, Strupler M, Boulesteix T, Godeau G, Schanne-Klein MC. Spectroscopic Analysis of Keratin Endogenous Signal for Skin Multiphoton Microscopy. 2005; Opt Express 13: 6268-6274.
8. Ramanujam N. Fluorescence Spectroscopy of Neoplastic and Non-neoplastic Tissues. Neoplasia 2000; 2: 89-117.
9. Leunig A, Rick K, Stepp H, Gutmann R, Alwin G, Baumgartner R, Feyh J. Fluorescence imaging and spectroscopy of 5-aminolevulinic acid induced Protoporphyrin IX for the dectection of neoplastic lesions in the oral cavity. The American Journal of Surgery 1996;172(6): 674-77.
10. Kostron H, Zimmermann A, Obwegeser A. mTHPC-mediated photodynamic detection for fluorescence-guided resection of brain tumors. Proc. SPIE 1998; 3262.
11. Tyrrell JS, Campbell SM, Curnow A. The relationship between protoporphyrin IX photobleaching during real-time dermatological methyl-aminolevulinate photodynamic therapy (MAL-PDT) and subsequent clinical outcome. Lasers Surg Med 2010; 42(7):613-19.
12. Wagnières GA, Star WM, Wilson BC. In vivo fluorescence spectroscopy and imaging for oncological applications. PhotochemPhotobiol 1998; 68(5): 603-32.
13. Borisova E, Avramov L, Laser System for Optical Biopsy and in vivo Study of the Human Skin. Proc. SPIE 2000; 4397: 405-09.
14. Bachmann L, Zezell D, da Costa Ribeiro A, Gomes L, Ito A. Fluorescence Spectroscopy of Biological Tissues. Appl Spectr Rev 2006; 41: 575-90.
15. Zemax company website. Zemax 2019.
16. Fischer RE, Tadic-Galeb B, Yoder PR. Optical System Design, New York. 2008.
17. Smith WJ. Modern Optical Engineering, 4th ed 2007.
18. Radiant, Zemax merge with backing from Evergreen Pacific, Bizjournal 2013.
19. Geary JM. Introduction to Lens Design: With Practical Zemax Examples. Willmann-Bel. 2002.
20. Moreno I, Sun CC. Modeling the radiation pattern of LEDs. Opt. Express 2008;16:1808-19.
21. Rollakanti KR, Kanick SC, Davis SC, Pogue BW, Maytin EV. Techniques for fluorescence detection of protoporphyrin IX in skin cancers associated with photodynamic therapy. Photonics Lasers Med 2013; 2(4):287-303.
22. Rajaram N, Kovacic D; Migden MF, Reichenberg JS, Nguyen TH, Tunnell JW. In vivo determination of optical properties and fluorophore characteristics of non-melanoma skin cancer. Proc SPIE 2009;716102: 1-9.
23. Bliznakova I, Borisova E, Avramov L. Laser and Light-Induced Autofluorescence Spectroscopy of Human Skin in Dependenceon Excitation Wavelengths. Acta Physica Polonica A 2007; 112:1131-
24. 36.
25. Wang I, Svanberg K, Andersson-Engels S, Berg R, Svanberg S. Photodynamic therapy of nonmelanoma skin malignancies with topical δ-amino levulinic acid: diagnostic measurements. Proc SPIE 1995; 2371:243-52.
26. Malzahn K, Dreyer T, Glanz H, Arens C. Autotuorescence endoscopy in the diagnosis of early laryngeal cancer and its precursor lesions. Laryngoscope 2002; 112(3): 488-93.
27. Zargi M, Fajdiga I, Smid L. Autofluorescence imaging in the diagnosis of laryngeal cancer. Eur Arch Otorhinolaryngol 2000; 257:17-23.
28. Arens C, Reussner D, Neubacher H, Woenckhaus J, Glanz H. Spectrometric measurement in laryngeal cancer 2006; Eur Arch Otorhinolaryngol 263(11):1001-1007.
29. Aboumarzouk O, Valentine R, Buist R, Ahmad S, Nabi G, Eljamel S, et al. Laser-induced autofluorescence spectroscopy: Can it be of importance in detection of bladder lesions? Photodiagnosis Photody Ther 2015; 12: 76-83.
30. Zhaojun N, Shu-Chi AY, LePalud M, Badr F, Tse F, et al. Optical Biopsy of the Upper GI Tract Using Fluorescence Lifetime and Spectra. Front Physiol 2020; 11:339.